




Quantum-Monte-Carlo–based functional for dysprosium dipolar systems

Raúl Bombín ^{1,2,*}, Viktor Cikojević ^{3,†}, Ferran Mazzanti,² and Jordi Boronat ²

¹*Institut des Sciences Moléculaires (ISM), Université de Bordeaux, 351 Cours de la Libération, 33405 Talence, France*

²*Departament de Física, Universitat Politècnica de Catalunya, Campus Nord B4-B5, 08034, Barcelona, Spain*

³*Faculty of Science, University of Split, Rudera Boškovića 33, HR-21000 Split, Croatia*



(Received 3 November 2023; accepted 23 February 2024; published 19 March 2024)

We present a quantum-Monte-Carlo–based density functional to describe droplet formation and supersolidity in dipolar systems. The usual Lee-Huang-Yang term, accounting for quantum correlations in the conventional extended Gross-Pitaevskii equation (eGPE), has been substituted by the correlation energy evaluated with quantum Monte Carlo. We demonstrate the ability of our functional to reproduce existing experimental data for the minimum critical number of atoms N_c required for droplet formation. N_c is a challenging quantity for theoretical predictions, and the eGPE provides only a qualitative description of it, mainly when it is applied to dysprosium. We also use our approach to characterize the BEC-supersolid transition. The quantum-Monte-Carlo–based functional can be easily implemented in any existing eGPE code, improving the description of dipolar systems without increasing the computational cost.

DOI: [10.1103/PhysRevA.109.033312](https://doi.org/10.1103/PhysRevA.109.033312)

I. INTRODUCTION

Ultracold dipolar systems made up of lanthanide atoms, mainly Dy [1], Er [2], or their mixtures [3], have been extensively studied in recent years (see Ref. [4] for an experimental review). The long-range and anisotropic nature of the dipolar interaction gives place to unique many-body phenomena such as the formation of ultradilute quantum droplets [5–7], the existence of supersolid phases [8–10], and, recently, the observation of anomalous temperature behavior [11,12]. State-of-the-art experiments provide unprecedented insight into this correlated regime. Some achievements in this respect are the measurement of the roton of the quasiparticle excitation spectrum [13], of collective excitations [14–16], and of the static structure factor, which has been used to characterize density fluctuations across the BEC-supersolid transition [17,18]. Recently, the first Bose-Einstein condensate of polar molecules has been observed [19], which would potentially give access to the study of new phenomena in dipolar systems.

The extended Gross-Pitaevskii equation (eGPE), which includes beyond-mean-field contributions to the Lee-Huang-Yang (LHY) form [20–22], has been extensively utilized to describe ultracold dipolar systems with remarkable success [23–29]. For instance, in Er systems, this theory allows us to describe the formation of droplets [6], supersolid phases [30], and also the excitation spectrum [13,30]. Similarly, for Dy atoms, the eGPE has been successfully applied to evaluate superfluid critical velocities [31] and collective excitations [14,15] and to describe striped states in oblate traps [32]. Despite these successes, some challenges still need to be addressed. It has been shown that incorporating the LHY

correction does not always result in an improvement, for instance, in the description of the roton minimum for Er systems [33]. More significantly, eGPE prediction of the critical (minimum) atom number to form a droplet in Dy systems is only qualitative [34]. In addition to this evidence, it is worth highlighting a fundamental drawback that affects the eGPE description in the regime where dipolar interaction dominates, namely, its dynamic instability in the long-wavelength limit.

Efforts to refine the eGPE description of ultracold dipolar systems have attempted to improve the description of quantum correlations [35–37] or to include thermal effects in the model [38,39]. An alternative approach consists of using quantum Monte Carlo (QMC), which evaluates exactly quantum correlations at all orders. However, its huge computational cost hinders the direct calculation of large systems containing a number of atoms $N > 10^4$. To tackle this limitation, models in which the experimental scattering length is rescaled to allow for the formation of small droplets have been used [40,41]. QMC calculations have also estimated the critical atom number for a small droplet ($N \sim 10^3$) [34]. The critical atom number arises from a subtle balance between dipolar attraction and quantum correlations, making it a challenging quantity to calculate. In the context of Bose-Bose mixtures, it has been shown that it is possible to avoid the QMC limitation in the number of atoms by constructing a density functional [42–45] with the same approach that was used previously in the study of liquid-⁴He drops [46,47]. Such a functional improves the description of quantum correlations, as it includes information from the QMC equation of state (EOS). In this work, we present a QMC-based density functional (DF) for dipolar systems. We specialize it to the study of Dy (Dy-DF). The Dy-DF is able to accurately reproduce the critical atom number for droplet formation, highlighting the potential of this approach for advancing our understanding of ultracold dipolar droplets. We also show that it can be applied to study

*raul.bombin@ehu.eus

†cikojevic.viktor@gmail.com

other relevant phenomena in Dy systems, such as the BEC-supersolid transition.

This paper is organized as follows. In Sec. II A we provide a description of the system that we study. In Secs. II B and II C the eGPE and path-integral ground-state (PIGS) methods are briefly described. PIGS results for the EOS are discussed in Sec. III. In Sec. IV we explain how we use the EOS obtained with the PIGS method to construct an eGPE-like density functional, which we call the dysprosium density functional. The accuracy of the Dy-DF is benchmarked using the available experimental data for the critical atom numbers of ^{162}Dy and ^{164}Dy droplets [34] in Sec. V. In Sec. VI we use the Dy-DF to study the BEC-supersolid transition, paying attention to the different observables. We also discuss the differences that emerge between the eGPE predictions and our theory. Finally, in Sec. VII some conclusions are summarized.

II. METHOD

A. The dipolar system

We study a system of N ^{162}Dy magnetic atoms with all the magnetic moments aligned along the Z direction in space. Such a system can be described by the following Hamiltonian:

$$\hat{H} = \hat{T} + \hat{V}_{\text{trap}} + \hat{V}_{2\text{B}}, \quad (1)$$

where $\hat{T} = -\sum_{i=1}^N \frac{\hbar^2 \hat{\nabla}_i^2}{2M}$ is the quantum kinetic-energy operator, with M being the mass of ^{162}Dy ; \hat{V}_{trap} is an external trapping potential; and $\hat{V}_{2\text{B}} = \hat{V}_{\text{SR}} + \hat{V}_{\text{dd}}$ is the two-body potential, consisting of a short-range Lennard-Jones potential \hat{V}_{SR} and a dipolar one \hat{V}_{dd} ,

$$V_{\text{SR}}(\mathbf{R}) = \sum_{i<j}^N \frac{C_{12}}{r_{ij}^{12}} - \frac{C_6}{r_{ij}^6}, \quad (2)$$

$$V_{\text{dd}}(\mathbf{R}) = \sum_{i<j}^N \frac{C_{\text{dd}}}{4\pi} \frac{1 - 3\cos^2\theta_{ij}}{r_{ij}^3}, \quad (3)$$

with $\mathbf{R} = (\mathbf{r}_1, \mathbf{r}_2, \dots, \mathbf{r}_N)$ being the set of $3N$ coordinates, \mathbf{r}_i being the position of the i th particle, $\mathbf{r}_{ij} = \mathbf{r}_i - \mathbf{r}_j$, (r_{ij}, θ_{ij}) being the polar coordinates of the vector \mathbf{r}_{ij} , and the C_i constants determining the strength of the different contributions to $V_{2\text{B}}$. The C_{12} value is chosen so that the total interaction potential has the desired s -wave scattering length a_s by solving the Lippmann-Schwinger equation associated with the T matrix of the full interaction [34], the van der Waals C_6 coefficient is fixed to the dysprosium experimental value [48], and $C_{\text{dd}} = \mu_0 m^2$, with μ_0 being the vacuum magnetic permeability and $m \approx 10\mu_B$ being the magnetic moment of ^{162}Dy . The trapping potential \hat{V}_{trap} is chosen to be a one-body harmonic potential. To evaluate the properties of a bulk, infinite system, the external potential is set to zero. The results presented in this work are in units of the dipolar length $r_0 = \frac{C_{\text{dd}}M}{4\pi\hbar^2}$ and the corresponding dipolar units of energy $\mathcal{E}_0 = \frac{\hbar^2}{Mr_0^2}$, unless otherwise stated.

B. The Gross-Pitaevskii equation

The Gross-Pitaevskii equation is a nonlinear differential equation that allows us to describe a bosonic system at zero

temperature. It provides a mean-field description assuming that almost all of the system remains in the condensate. When quantum correlations in the LHY form are included, it is usually referred to as the extended Gross-Pitaevskii equation, which in the case of a dipolar system reads [21,22,24–26]

$$i\hbar \frac{\partial}{\partial t} \Psi(\mathbf{r}, t) = \mu \Psi(\mathbf{r}, t), \quad (4)$$

where Ψ is the one-body mean-field wave function and μ is the chemical potential, which reads

$$\mu = -\frac{\hbar^2 \nabla^2}{2M} + V_{\text{trap}} + g|\Psi|^2 + \Gamma_{\text{QF}}|\Psi|^3 + \Phi_{\text{dd}}, \quad (5)$$

with $g = 4\pi\hbar^2 a_s/M$ being the coupling constant and $\Gamma_{\text{QF}}|\Psi|^3$ being the LHY correction including quantum correlations [20–22],

$$\Gamma_{\text{QF}}|\Psi|^3 = \frac{32g\sqrt{a_s^3}}{3\sqrt{\pi}} Q_5(\varepsilon_{\text{dd}})|\Psi|^3, \quad (6)$$

with $\varepsilon_{\text{dd}} = a_{\text{dd}}/a_s$, $a_{\text{dd}} = r_0/3 = \frac{C_{\text{dd}}M}{12\pi\hbar^2}$, and $Q_5(\varepsilon_{\text{dd}}) = \frac{1}{2} \int_0^\pi d\alpha \sin\alpha [1 + \varepsilon_{\text{dd}}(3\cos^2\alpha - 1)]^{5/2}$; the last term in Eq. (5) is a nonlocal term that accounts for the dipolar interaction,

$$\Phi_{\text{dd}}(\mathbf{r}) = \int d\mathbf{r}' V_{\text{dd}}(\mathbf{r} - \mathbf{r}') |\Psi(\mathbf{r}', t)|^2. \quad (7)$$

At zero temperature, the chemical potential of Eq. (4) is related to the internal energy U through the thermodynamic relation

$$\mu = \left(\frac{\partial U}{\partial N} \right)_V = \frac{\rho}{N} \left(\frac{\partial U}{\partial \rho} \right)_V = \left(\frac{\partial \mathcal{E}}{\partial \rho} \right)_V, \quad (8)$$

where $V = N/\rho$ is the volume of the system, ρ is the density, and $\mathcal{E} = \rho U/N$ is the energy per unit of volume or the energy density.

C. Path-integral ground state

PIGS is a stochastic method that allows us to evaluate the properties of quantum many-body systems at zero temperature [49–52]. In the case of bosonic systems it provides exact results within some statistical uncertainty. The method allows us to sample the ground state of the system ϕ_0 by propagating in imaginary time τ a many-body trial wave function $\Phi_T(\mathbf{R}, \tau)$,

$$\phi_0 = \lim_{\tau \rightarrow \infty} \Phi(\mathbf{R}, \tau) = \int \lim_{\tau \rightarrow \infty} d\mathbf{R}' G(\mathbf{R}, \mathbf{R}'; \tau) \Phi_T(\mathbf{R}', 0), \quad (9)$$

where $G(\mathbf{R}, \mathbf{R}'; \tau)$ is the propagator operator in the imaginary-time interval τ .

In general, the many-body propagator is unknown, and instead, one uses a short-time approximation $\delta\tau$ and iterates Eq. (9). To achieve large imaginary times, a set of M_b intermediate coordinates (beads) $\{\mathbf{R}_i\}$ is introduced in Eq. (9), which

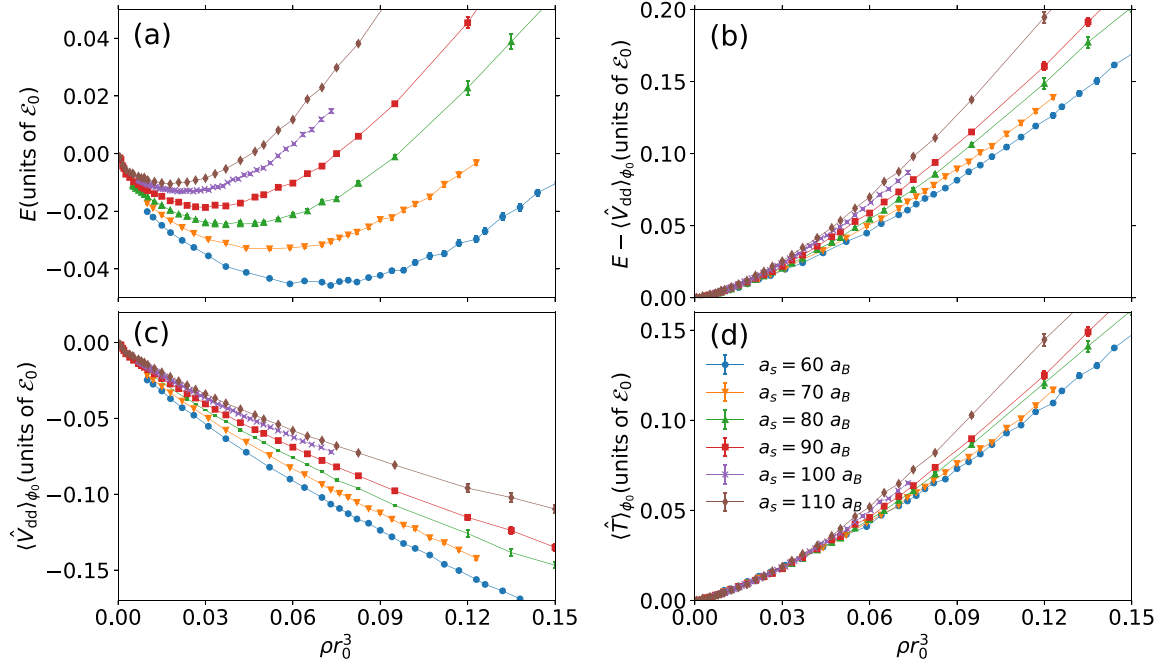


FIG. 1. PIGS results for (a) energy per particle E , (b) energy per particle without a dipolar contribution $E - \langle \hat{V}_{\text{dd}} \rangle_{\phi_0}$, (c) dipolar energy per particle $\langle \hat{V}_{\text{dd}} \rangle_{\phi_0}$, and (d) correlation energy per particle $\langle \hat{T} \rangle_{\phi_0}$ as a function of the density ρr_0^3 . Results are shown for different values of the scattering length. Lines are guides to the eye.

takes the form

$$\phi_0(\mathbf{R}_{N_b+1}) = \lim_{\substack{\delta\tau \rightarrow 0 \\ N_b \rightarrow \infty \\ \tau \rightarrow \infty}} \int \prod_{i=1}^{M_b} d\mathbf{R}_1 d\mathbf{R}_2 \cdots d\mathbf{R}_{N_b} \times G(\mathbf{R}_{i+1}, \mathbf{R}_i; \delta\tau) \Phi_{\text{T}}(\mathbf{R}_1, 0). \quad (10)$$

The method guarantees that the ground state is reached for sufficiently small $\delta\tau$ and sufficiently large N_b , with $\tau = \delta\tau M_b \rightarrow \infty$, as long as the trial wave function is not orthogonal to the actual ground state of the system. We use a fourth-order Chin action propagator [53,54], and permutations are sampled with the efficient worm algorithm [55,56]. In the calculations presented in this work the trial wave function is chosen to be a constant, which has been demonstrated to be sufficient even for correlated systems such as ^4He [57].

III. EQUATION OF STATE

The bulk dipolar system is simulated by considering $N = 512$ ^{162}Dy atoms in a cubic box of length $L = \sqrt{N/\rho}$ with fixed density ρ and periodic boundary conditions. We consider values of the scattering length that cover the whole range of state-of-the-art experiments with ^{162}Dy and ^{164}Dy atoms: $a_s = \{60, 70, 80, 90, 101.57, 110\}a_B$, with a_B being the Bohr radius. The energy per particle $E(\rho)$ of Fig. 1(a) corresponds to the EOS of a liquid; i.e., it exhibits a minimum in the energy per particle at the equilibrium density ρ_{eq} . The values of the equilibrium density ρ_{eq} and the binding energy per particle E_b are shown in Table I. For small values of the scattering length the dipolar interaction dominates, and the system forms a denser liquid with a larger binding energy. The formation of

the liquid arises from the balance between dipolar attraction and the repulsion coming from quantum correlations.

To give further insight into the energetic balance of the dipolar system, in Fig. 1(b) the dipolar energy contribution to the energy per particle $\langle \hat{V}_{\text{dd}} \rangle_{\phi_0}$ is subtracted from E , and Fig. 1(c) plots $\langle \hat{V}_{\text{dd}} \rangle_{\phi_0}$. In the above expressions $\langle \hat{O}_{\text{dd}} \rangle_{\phi_0}$ stands for the expectation value of the operator \hat{O} in the ground state of the system. Results in Figs. 1(b) and 1(c) show that the binding of the dipolar systems is entirely caused by the dipolar attraction. In this respect, it is worth remarking that E arises from a large cancellation between these two terms, which hints at the subtle energetic balance that exists between short-range repulsion, quantum correlation energy, and dipolar interaction in the ultracold regime. To elucidate the role that quantum correlations play, in Fig. 1(d) we show explicitly the kinetic (correlation) energy $\langle \hat{T} \rangle_{\phi_0}$. Comparing Figs. 1(b) and 1(d) clearly shows that quantum correlations dominate the repulsive contribution to E and thus play a major role in the stabilization of the system. This is a well-known fact in the ultracold-gas community, although an accurate quantitative

TABLE I. PIGS results for the equilibrium density ρ_{eq} and binding energy per atom E_b at that density for a bulk ^{162}Dy system.

a_s/a_B	$\rho_{\text{eq}} r_0^2$	E_b/\mathcal{E}_0
60.00	0.068	-0.045
70.00	0.051	-0.033
80.00	0.039	-0.024
90.00	0.029	-0.018
101.57	0.023	-0.013
110.00	0.018	-0.011

evaluation of quantum correlations for realistic experimental parameters has been lacking. From the theoretical side, the inclusion of quantum correlations in the form of a LHY term in the Gross-Pitaevskii equation allows us to stabilize the droplets and has allowed us to describe the mechanism of droplet formation (see, for example, Ref. [23]). In the next section we construct an eGPE density functional by replacing the LHY term by the quantum correlations evaluated with PIGS.

IV. DIPOLAR DENSITY FUNCTIONAL

The eGPE equation introduced in Sec. II B can be derived from the minimization of the following functional for the internal energy by imposing the usual energy variational principle $\delta(E - \mu N) = 0$ [43,58]:

$$\begin{aligned} U_{\text{LHY}} &= \int \mathcal{E}_{\text{LHY}}[\Psi] d\mathbf{r} \\ &= \int \left[\frac{\hbar^2}{2m} |\nabla \Psi|^2 + V_{\text{trap}} |\Psi|^2 + \frac{1}{2} g |\Psi|^4 + \frac{2}{5} \Gamma_{\text{QF}} |\Psi|^5 \right. \\ &\quad \left. + \frac{1}{2} \int d\mathbf{r}' V_{\text{dd}}(\mathbf{r} - \mathbf{r}') |\Psi(\mathbf{r}', t)|^2 |\Psi(\mathbf{r}, t)|^2 \right] d\mathbf{r}. \end{aligned} \quad (11)$$

Using the local-density approximation (LDA), that is, setting $\rho = |\Psi|^2$, one can rewrite the LHY-DF \mathcal{E}_{LHY} as

$$\begin{aligned} \mathcal{E}_{\text{LHY}}[\rho] &= \frac{\hbar^2}{2m} |\nabla \sqrt{\rho}|^2 + V_{\text{trap}} \rho + \frac{1}{2} g \rho^2 + \frac{2}{5} \Gamma_{\text{QF}} \rho^{5/2} \\ &\quad + \frac{1}{2} \int d\mathbf{r}' V_{\text{dd}}(\mathbf{r} - \mathbf{r}') \rho(\mathbf{r}') \rho(\mathbf{r}). \end{aligned} \quad (12)$$

Note that in the case of a uniform bulk system [$\rho(r) \sim \text{const}$, $V_{\text{trap}} = 0$], the first two terms and the last one in Eq. (12) vanish, and one obtains a functional for the energy density of the uniform dipolar bulk system that reads

$$\mathcal{E}_{\text{LHY}}^{\text{BULK}}[\rho] = \frac{1}{2} g \rho^2 + \frac{2}{5} \Gamma_{\text{QF}} \rho^{5/2}. \quad (13)$$

On the other hand, using the PIGS method, one can compute the EOS of the dipolar bulk system from the energy per particle $E_{\text{QMC}}(\rho) = U_{\text{QMC}}(\rho)/N$ for a given value of the s -wave scattering length. For the system described by the Hamiltonian in Eq. (1) it reads

$$E_{\text{QMC}}^{\text{BULK}}(\rho = |\phi_0|^2) = \langle \hat{T} \rangle_{\phi_0} + \langle \hat{V}_{\text{SR}} \rangle_{\phi_0} + \langle \hat{V}_{\text{dd}} \rangle_{\phi_0}, \quad (14)$$

which is a sum of three contributions: correlation energy, short-range interaction, and dipolar interaction. As has been done in the context of helium [46,47] and Bose-Bose mixtures [42–44], one could study the nonuniform system, e.g., confined BEC, droplets, etc., under the LDA approximation with a functional of the form

$$\mathcal{E}_{\text{QMC}}[\rho] = \frac{\hbar^2}{2m} |\nabla \sqrt{\rho}|^2 + V_{\text{trap}} \rho + \mathcal{E}_{\text{QMC}}^{\text{BULK}}[\rho], \quad (15)$$

with $\mathcal{E}_{\text{QMC}}^{\text{BULK}} = \rho E_{\text{QMC}}^{\text{BULK}}$. However, it is important to note that the functional in Eq. (15) is isotropic, and thus, it is not a good functional to describe dipolar systems, in which the anisotropy introduced by the dipolar interaction plays a major role. In the LHY functional the anisotropy is naturally included in the nonlocal dipolar potential V_{dd} .

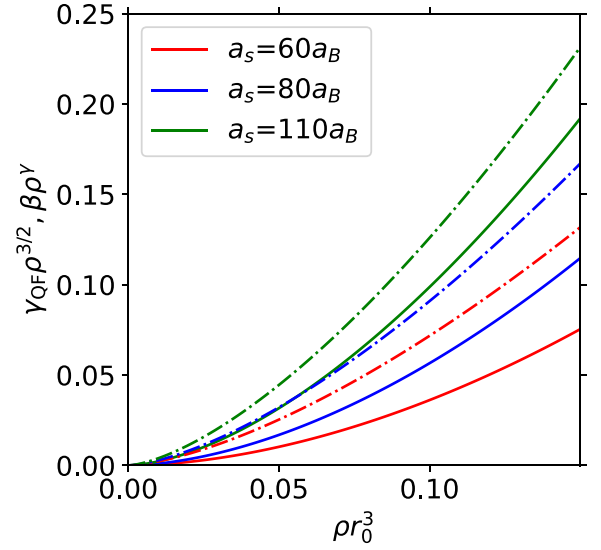


FIG. 2. Solid and dashed lines show the quantum fluctuation terms of the Dy-DF and the LHY-DF as a function of the density for different values of the scattering length, respectively. In the former case it corresponds to the nonlinear term ($\beta \rho^\gamma$) in Eq. (16), and in the latter it corresponds to Eq. (6).

In this work we construct an eGPE-like density functional for dysprosium dipolar systems, replacing the quantum fluctuations term in Eq. (12) with the nonlinear contribution to the quantum kinetic energy. To do so, we fit $\langle \hat{T} \rangle_{\phi_0}(\rho)$ evaluated with PIGS with a function of the form of (13). Explicitly,

$$\langle \hat{T} \rangle_{\phi_0} = \alpha_{\text{QMC}} \rho + \beta_{\text{QMC}} \rho^{\gamma_{\text{QMC}}}. \quad (16)$$

This approach implies assuming that the linear term in the usual eGPE description is accurate enough and that only a modification in the quantum correlation term is needed in order to include beyond-LHY effects. In a different approach, small modifications to the LHY-DF were proposed in order to improve the accuracy in the description of quantum dipolar systems (see Ref. [37]). Due to the stochastic nature of the PIGS method, statistical uncertainties are present in our data. Details of the fitting procedure are given in Appendix A, and the specific values of $\{\beta(a_s), \gamma(a_s)\}$ are summarized in Table II. To facilitate the use of the Dy-DF for any value of a_s in the interval $a_s \in [60, 110]a_B$, the values $\{\beta(a_s), \gamma(a_s)\}$ are interpolated in terms of a_s with a linear function. The parameters for these fits are summarized in Table III in Appendix B. This interpolation allows us to use the Dy-DF by introducing a minimal correction in the LHY term in Eq. (12): $\frac{2}{5} \Gamma_{\text{QF}} |\Psi|^3 \rightarrow \beta_{\text{QMC}} |\Psi|^{\gamma_{\text{QMC}}+1}$; thus, its implementation in any existing eGPE code is straightforward. It is worth remarking that the computational cost of the Dy-DF is exactly the same as that of the LHY-DF one. The quality of this approach is discussed in the next section.

In Fig. 2 we compare the quantum correlation term of the Dy-DF with that of the LHY-DF as a function of density. The values of the scattering length that are considered ($a_s = 60a_B$, $80a_B$, and $110a_B$) cover the whole range of experimental values. As can be observed in Fig. 2, the Dy-DF is always less repulsive than the LHY one. Differences between the two functionals are larger when the scattering length is smaller,

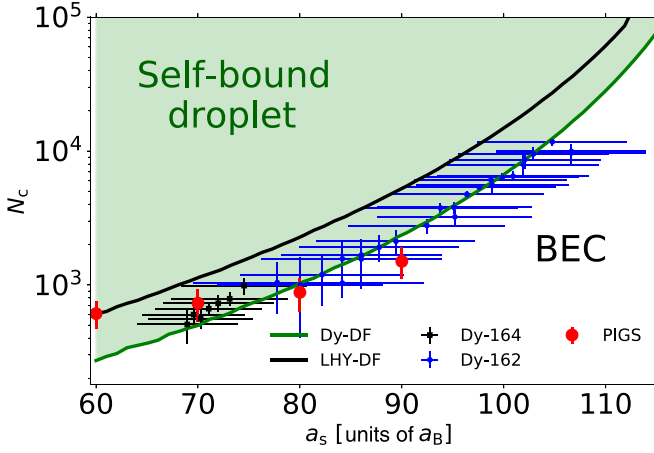


FIG. 3. Critical atom number to form a dysprosium dipolar droplet. Green and black lines are Dy-DF and LHY-DF predictions, respectively. Black squares and blue dots are experimental measurements for ^{164}Dy and ^{162}Dy , respectively [34]. Red points are obtained by direct calculations of quantum droplets with PIGS [34].

which hints at a large beyond-mean-field correction when the dipolar interaction dominates.

V. CRITICAL ATOM NUMBER

The resulting Dy-DF is less repulsive than the LHY one; thus, it is expected to predict a smaller critical atom number for droplet formation. As shown in Fig. 3, the Dy-DF (green line) reproduces with remarkable accuracy the available experimental data for the critical atom number of Dy atoms (black and blue dots). This improvement over the LHY-DF description (black line), which systematically overestimates this quantity, highlights the accuracy of the Dy-DF functional. Although our functional is designed for ^{162}Dy , it also reproduces the experimental data for ^{164}Dy , which suggests a minor isotopic effect in dysprosium droplets (note that the difference in mass and magnetic moment between the two atoms is about 1%).

For the sake of comparison, we also include in Fig. 3 the PIGS results obtained by direct computation of small dipolar droplets [34]. PIGS results are compatible with the experimental values in the range $a_s \in [70, 90]a_B$, where both PIGS calculations and experimental data are available. However, for $a_s = 60a_B$, the Dy-DF and PIGS predictions are in clear disagreement. This difference can be attributed, at least in part, to the different methods used in both theories to estimate N_c . With Dy-DF, N_c is calculated as the atom number for which the radius of the dipolar droplet starts to diverge in the absence of a trapping potential. This facilitates the direct comparison with experiments, where the same criteria to determine N_c are used. In the case of the direct PIGS calculations, using the size criteria is unfeasible. In that case, N_c was determined as the minimum atom number for which $E < 0$ [34]. Appendix B shows that the energy criterion provides critical atom numbers that are slightly larger than the ones obtained with the droplet-radius criterion.

VI. BEC-SUPERSOLID TRANSITION

The BEC-supersolid transition, which arises in dipolar systems trapped in a quasi-one-dimensional configuration, has been studied extensively [8,10,11,15,16,18,30,59,60]. Here, we focus on the experimental setup of Refs. [9,10,16], where the trapping frequencies are $\omega_{x,y,z} = 2\pi(18.5, 53, 81)$ Hz and the dipoles are aligned along the Z axis with $N = 3.5 \times 10^4$ atoms. Similar to what happens with droplet formation, the modulational instability that gives rise to the supersolid phase emerges from the balance between dipolar attraction and quantum correlations. Thus, the supersolid window, namely, the interval of scattering-length values in which this phase is observed, is quite sensitive to the details of the theoretical description. In this respect, as previously mentioned, the Dy-DF is more attractive than the usual LHY-DF, so the supersolid phase is expected to appear for larger values of the scattering length (lower $\varepsilon_{dd} = a_{dd}/a_s$).

Figures 4(a) and 4(c) show the density profiles $\rho(x)$ along the X direction, where the confinement is weaker, calculated with Dy-DF and LHY-DF, respectively. The Dy-DF (LHY-DF) predicts a BEC state for $\varepsilon_{dd} < 1.27$ (1.37), while for larger values of ε_{dd} , a density stability emerges, resulting in a modulated $\rho(x)$ distribution. Both functionals predict the formation of two large clusters in the center of the trap accompanied by two smaller satellite ones. As ε_{dd} is further increased, the intercluster density vanishes, and a transition to a third regime occurs, where only two insulating droplets are present. This intermediate state is termed supersolid, as it exhibits spatial order and phase coherence simultaneously. Similarly, the system of insulating droplets constitutes a solid of droplets.

To characterize the transition between the three aforementioned regimes, namely, BEC, supersolid, and solid, we evaluate the superfluid fraction f_s and the intensity of the density modulations. Leggett's upper bound [61,62] for the superfluid fraction is given by

$$f_s \leq (2L)^2 \left[\left(\int_{-L}^L dx \rho(x) \right) \left(\int_{-L}^L \frac{dx}{\rho(x)} \right) \right]^{-1}, \quad (17)$$

where the distance $2L$ encloses the central part of the trap, where the droplets form. Recently, the quality of Leggett's upper bound was studied, showing that it provides accurate results for dilute gases [63]. To evaluate the spatial structure of the modulated phases, we compute the contrast C between the height of the central peaks and the depletion of density around them as

$$C = \frac{\max[\rho(x)] - \min[\rho(x)]}{\max[\rho(x)] + \min[\rho(x)]}. \quad (18)$$

The superfluid fraction and contrast are computed for the ground state predicted by the LHY and Dy-DF functionals. As we are dealing with a trapped system, we compute Eqs. (17) and (18) in the central region of the trap, which is delimited by the gray vertical lines in Figs. 4(a) and 4(c).

Figures 4(b) and 4(d) summarize the Dy-DF and LHY-DF results for the superfluid fraction and the contrast as a function of ε_{dd} . The critical value of ε_{dd} at which the transition from a BEC to a supersolid phase occurs is $\varepsilon_{dd}^{\text{crit}} = 1.28$ (1.38) for the Dy-DF (LHY-DF). Below this critical value, $f_s = 1$ (and

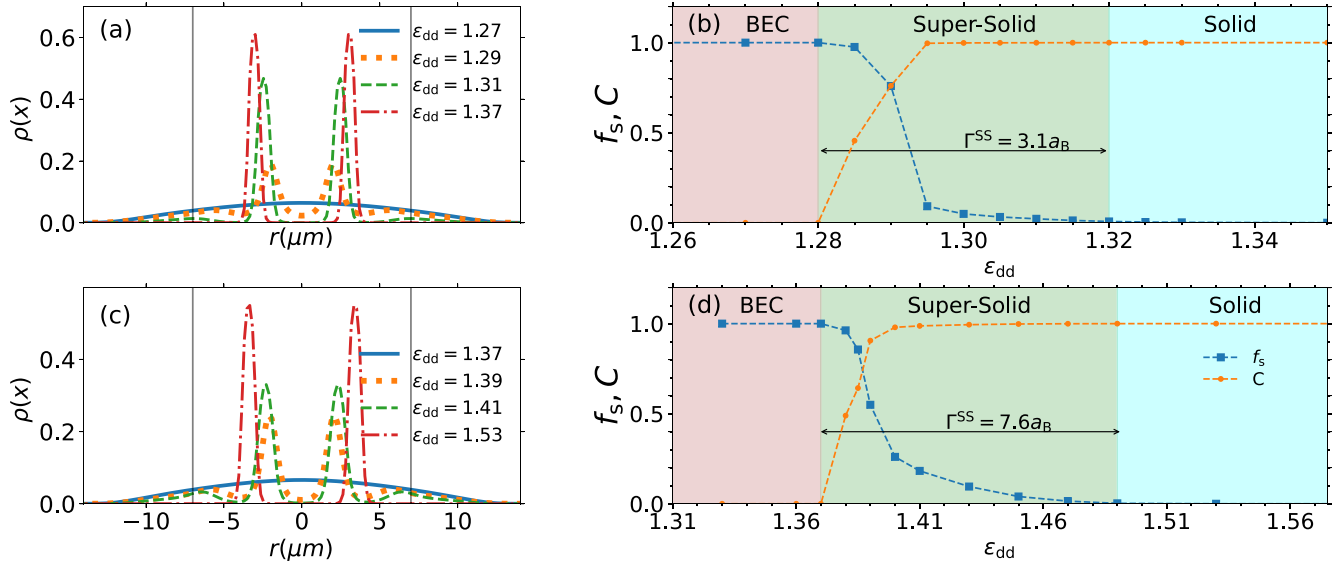


FIG. 4. Properties evaluated along the BEC-supersolid transition with the Dy-DF (top) and LHY (bottom) functionals. (a) and (c) contain the density profiles along the X direction for different values of ε_{dd} . (b) and (d) depict the superfluid fraction f_s [blue squares; see Eq. (17)] and contrast C [orange circles; see Eq. (18)] computed with the LHY-DF (left) and Dy-DF (right) as a function of ε_{dd} . Dashed lines are guides to the eye. Note that the scales in (b) and (d) are different. Gray vertical lines in (a) and (c) delimitate the region where f_s and C are computed.

$C = 0$). In the supersolid region, the superfluid density rapidly drops to values lower than 1, and the contrast increases. Note that values of C close to 1 are obtained before the superfluid signal completely vanishes. For $\varepsilon_{dd} > 1.32$ (1.48), Dy-DF (LHY-DF) predicts an insulating droplet array ($f_s = 0$ and $C = 1$).

In Ref. [16], the axial mode frequencies were measured across the BEC-supersolid transition in the configuration that we study here. The authors showed that two modes can be excited in the supersolid regime. The high-energy one is related to the lattice-site vibrations, while the lower one is related to the droplet-coherence oscillations. To compute the axial mode frequencies, we introduce a perturbative potential $H_{\text{pert}} = -\lambda x^2$, with λ being a small parameter. Once it is equilibrated, the perturbation is switched off, and the solution is propagated in real time, computing $\langle x^2(t) \rangle$. The axial mode frequencies are obtained by performing a Fourier transform of $\langle x^2(t) \rangle$.

The axial mode frequencies computed with the Dy-DF are shown in Fig. 5 (blue and brown circles). For $\varepsilon_{dd} < 1.27$, the system is in the BEC regime, and a single frequency is observed ($\omega/\omega_x \approx 1.47$). In the region $1.27 < \varepsilon_{dd} < 1.34$, where the system is modulated (see Fig. 4), two frequencies appear in the Fourier spectra. The magnitude of the higher-energy mode is larger than the value of the single mode in the BEC regime, while the superfluid mode decreases quickly with ε_{dd} and vanishes for $\varepsilon_{dd} > 1.34$. This ending point signals the transition from the supersolid state to the normal solid one. In this phase, only the upper frequency branch appears with a value $\omega/\omega_x \approx 2.0$.

In Fig. 5, we also show the experimental measurement and LHY-DF prediction for these two frequencies as reported in Ref. [16]. Note that the uncertainty in the measurement of a_s , which can be of the order of $10a_B$, results in an uncertainty of

0.12 in the value of ε_{dd} . More refined experimental measurements would be needed in order to determine precisely the supersolid transition point and to discern between the Dy-DF and LHY-DF predictions. Despite that, let us analyze the differences between the two functionals. In the BEC regime both functionals reproduce the experimental value $\omega_x/\omega \approx 1.47$ within a 3% of error. In the supersolid regime the behavior of the LHY-DF modes is similar to that of the Dy-DF, but it is noticeable that the interval in which the two frequencies appear is larger in the former case. The LHY superfluid frequency is

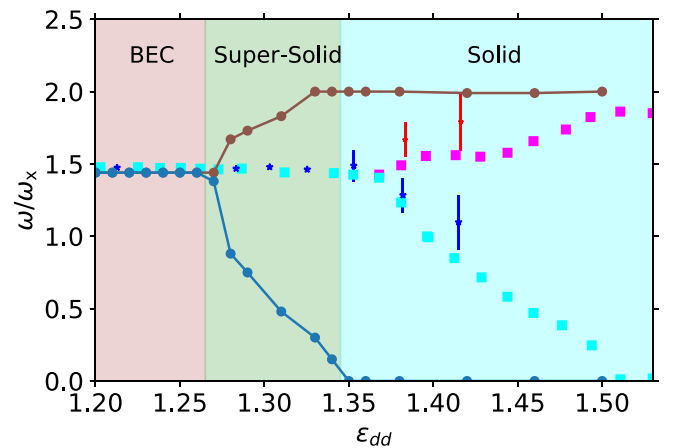


FIG. 5. Axial mode frequencies in units of the trapping frequency ω_x across the BEC-to-supersolid transition for the trap system of Fig. 4. Circles connected by brown and blue lines are the Dy-DF predictions for the superfluid and solid frequencies. Blue and red points with error bars are the corresponding experimental measurements of Ref. [16]. Pink and blue squares are LHY results from Ref. [16].

close to the experimental one, but it underestimates the value of the lattice frequency. On the contrary, the Dy-DF prediction reproduces the frequency of the experimental lattice mode but underestimates the superfluid one. In the solid regimes the functionals predict a single frequency mode at $\omega/\omega_x = 2.00, 1.85$ for Dy-DF and LHY-DF, respectively.

An important difference between the two theoretical approaches is the difference in the width of the supersolid window in terms of the scattering length Γ^{SS} . The experimental estimation of the supersolid window for the same setup given in Ref. [10] was obtained by measuring *in situ* modulations and phase coherence between the different drops. The reported value is $\Gamma_{exp}^{SS} \approx 6a_B$. It is worth noticing that for both the Dy-DF and LHY-DF the prediction for Γ^{SS} is rather different if it is evaluated in terms of the values of f_s from Fig. 4 or the excitation spectra in Fig. 5. The second choice provides slightly larger values. The LHY-DF prediction for the supersolid window attending to f_s is $\Gamma_{LHY}^{SS} \approx 7.6a_B$, while the width of the interval in which two frequencies appear in the Fourier spectra in Fig. 5 is $8.8a_B$. In the case of the Dy-DF functional, the first (second) criterion gives $\Gamma_{Dy-DF}^{SS} \approx 3.1a_B$ ($5.3a_B$). Thus, the experimental measurement of Ref. [10] lies in between the results of the two functionals.

VII. DISCUSSION AND CONCLUSIONS

In summary, the dysprosium density functional that we presented in this work allows us to study Dy dipolar systems and the rich phenomena that they exhibit, such as droplet formation and supersolidity. We evaluated the properties of a bulk dipolar system made of ^{162}Dy atoms using first-principles quantum Monte Carlo. The functional was constructed under the local-density approximation by replacing the usual LHY term, which accounts for quantum correlations in the standard eGPE, with exact quantum correlations computed with QMC. To benchmark our functional, we computed the minimum (critical) atom number that is needed to form a droplet and showed that our theory reproduces the experimental measurements for this quantity in spite of the large uncertainties in the experimental determination of the scattering lengths. The critical atom number is a challenging observable from a theoretical point of view, as it arises from a delicate energy balance between two similar (and opposite-sign) quantities: the interatomic dipolar inter-

action and the contribution from quantum correlations. On the contrary, the LHY theory provides only a qualitative description of the droplet formation mechanism. Furthermore, we demonstrated the suitability of our functional to study the BEC-to-supersolid phase transition and discussed the small discrepancies that appear between the LHY theory and our functional. Importantly, the Dy-DF improves the accuracy of the widely used eGPE without increasing the computational cost. A lot of work has been done in the last few years to achieve condensates of dipolar molecules that have a large electric moment [64–67] and for which the intermolecular interaction is known with spectroscopic precision [68]. Recently, the formation of a Bose-Einstein condensate of dipolar molecules was reported [19], what constitutes a breakthrough that opens the door to study new physics in dipolar systems. We hope that the approach presented here will also be useful for the study of such condensates of dipolar molecules in the future.

The code to reproduce the fitting procedure is available from GitHub [69].

ACKNOWLEDGMENTS

We acknowledge T. Pfau and F. Böttcher for sharing with us the experimental data set for the critical atom number. We acknowledge financial support from Ministerio de Ciencia e Innovación MCIN/AEI/10.13039/501100011033 (Spain) under Grant No. PID2020-113565GB-C21 and from AGAUR-Generalitat de Catalunya Grant No. 2021-SGR-01411. R.B. acknowledges the European Union-NextGenerationEU, Ministry of Universities and Recovery, Transformation and Resilience Plan, through a call from Polytechnic University of Catalonia. R.B. further acknowledges funding from the European Union’s Horizon 2020 research and innovation programme under the Marie Skłodowska-Curie Grant Agreement No. 101034379.

APPENDIX A: FITTING PROCEDURE

The Dy-DF is constructed by replacing the LHY term, accounting for quantum correlations in the eGPE description, with the nonlinear contribution of the quantum kinetic energy, namely, quantum correlations. Although QMC provides us with exact results for bosonic systems, they are accompanied by a certain variance due to the stochastic nature of the method. To deal with it we make linear fits of $\langle \hat{T}_\phi \rangle_0$

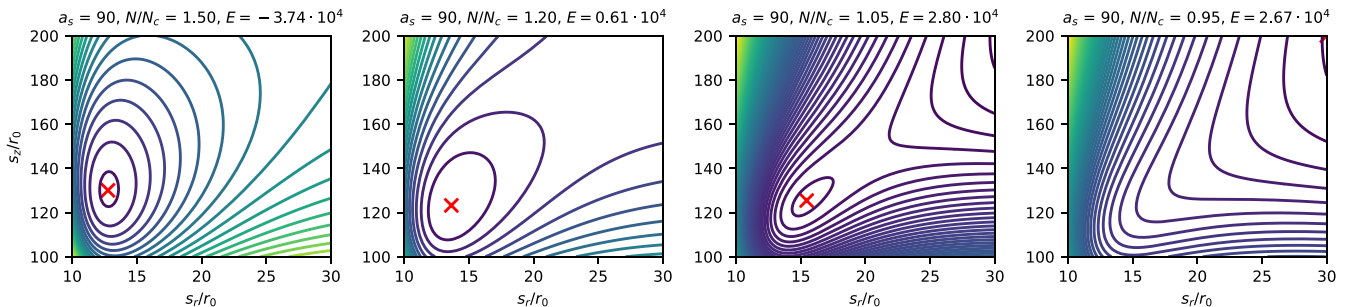


FIG. 6. Energy landscape in terms of the Gaussian widths σ_z and σ_r for $a_s = 90a_0$ and various N/N_c ratios. The red markers indicate local minima. The values of the N/N_c ratios and the energy of the local minima are indicated on each panel.

TABLE II. Parameters for the quantum fluctuation term in the energy per particle at the LHY-DF level and as extracted from Eq. (16) to construct the Dy-DF. In the LHY case $\beta_{\text{LHY}} = \frac{2}{3}\Gamma_{\text{QF}}$, and $\gamma_{\text{LHY}} = 1.5$ [see Eq. (5)]. The Dy-DF values are obtained after averaging different fits, where the fitting interval of the PIGS data is slightly varied and the number in parentheses corresponds to the standard deviation; see the text for details.

a_s/a_B	LHY-DF		Dy-DF	
	$\beta = \frac{2}{3}\Gamma_{\text{QF}}[\mathcal{E}_0 r_0^3]$	γ	$\beta[\mathcal{E}_0 r_0^3]$	γ
60	2.269	1.5	3.0(3)	2.00(6)
70	2.562	1.5	1.93(15)	1.53(7)
80	2.876	1.5	3.35(8)	1.80(1)
90	3.215	1.5	3.3(9)	1.65(13)
101.57	3.583	1.5	3.4(5)	1.62(7)
110	3.984	1.5	5.0(7)	1.73(6)

a function of the form $\alpha\rho + \beta\rho^\gamma$ in different intervals of the density $[\rho_{\text{min}}, \rho_{\text{max}}]$ around the equilibrium density ρ_{eq} (see Table I). We consider all the possible combinations of ρ_{min} and ρ_{max} such as $\rho_{\text{min}}/\rho_{\text{eq}} \in [0.4, 0.7]$ and $\rho_{\text{max}}/\rho_{\text{eq}} \in [1.5, 2.5]$, considering increments of 0.1 and 0.3, respectively. The resulting mean values of β and γ are listed in Table II, with their variance indicated in parentheses. Note that the parameter α in Eq. (16) is not used for the construction of the functional and thus is not given in Table II to avoid confusion. The values of α in the fit of the kinetic energy are 249(6), 760(13), 924(15), 2818(695), 8715(1537), 21185(3407) for $a_s = 60a_B, 70a_B, 80a_B, 90a_B, 101a_B, 110a_B$, respectively.

We perform a linear interpolation of the values of β and γ in Table II to create a functional dependence on a_s . The parameters for the linear fits of β and γ in terms of a_s are given in Table III. This procedure allows to use the Dy-DF for any value of the scattering length in the interval $[60, 110]a_B$. It also allows to implement straightforwardly the Dy-DF in existing eGPE code.

TABLE III. The parameters β and γ from Table II are interpolated in terms of the scattering length a_s with a linear function $ma_s + n$. The values of m and n for the two parameters are given.

	$m[\mathcal{E}_0 r_0^2]$	$n[\mathcal{E}_0 r_0^3]$
β	0.03935	-0.01422
	$m[r_0^{-1}]$	n
γ	-0.003434	2.0182

APPENDIX B: EVALUATION OF CRITICAL ATOM NUMBER

We evaluate the critical atom number within the density-functional formalism. To this end, we employ a Gaussian ansatz parametrized in the radial and axial directions with the widths s_r and s_z , respectively. The normalized density of a given Gaussian wave function is given by

$$\rho(r, z) = \frac{N}{\sqrt{\pi s_r^2 s_z}} e^{-\frac{r^2}{2s_r^2} - \frac{z^2}{2s_z^2}}, \quad (\text{B1})$$

where N is the total number of atoms. With this ansatz, the energy of the system can be calculated after plugging it into Eq. (12). We define the critical atom number as the number of atoms under which the local minimum of the energy landscape $E(s_r, s_z)$ vanishes. Notice that the energy can be positive, signaling a metastable state. To give further insight into this, in Fig. 6, we plot the energy landscape for $a_s = 90a_0$ for various N/N_c ratios. For this purpose, the Dy-DF parameters taken from Table III are used. It is evident that the energy of a local minimum decreases with a decrease in N/N_c . Notably, at around $N/N_c = 1.2$, the energy becomes positive, meaning that the global minimum vanishes for finite s_r and s_z values. Despite this, a local minimum persists, indicating the presence of a metastable minimum. This metastable state ceases to exist when N/N_c drops below 1. The red markers in Fig. 6 serve to highlight the points of local minima. Obviously, for $N/N_c < 1$ no local minima are observed.

- [1] M. Lu, N. Q. Burdick, S. H. Youn, and B. L. Lev, Strongly dipolar Bose-Einstein condensate of dysprosium, *Phys. Rev. Lett.* **107**, 190401 (2011).
- [2] K. Aikawa, A. Frisch, M. Mark, S. Baier, A. Rietzler, R. Grimm, and F. Ferlaino, Bose-Einstein condensation of erbium, *Phys. Rev. Lett.* **108**, 210401 (2012).
- [3] A. Trautmann, P. Ilzhöfer, G. Durastante, C. Politi, M. Sohmen, M. J. Mark, and F. Ferlaino, Dipolar quantum mixtures of erbium and dysprosium atoms, *Phys. Rev. Lett.* **121**, 213601 (2018).
- [4] L. Chomaz, I. Ferrier-Barbut, F. Ferlaino, B. Laburthe-Tolra, B. L. Lev, and T. Pfau, Dipolar physics: A review of experiments with magnetic quantum gases, *Rep. Prog. Phys.* **86**, 026401 (2023).
- [5] M. Schmitt, M. Wenzel, F. Böttcher, I. Ferrier-Barbut, and T. Pfau, Self-bound droplets of a dilute magnetic quantum liquid, *Nature (London)* **539**, 259 (2016).
- [6] L. Chomaz, S. Baier, D. Petter, M. J. Mark, F. Wächtler, L. Santos, and F. Ferlaino, Quantum-fluctuation-driven crossover from a dilute Bose-Einstein condensate to a macrodroplet in a dipolar quantum fluid, *Phys. Rev. X* **6**, 041039 (2016).
- [7] I. Ferrier-Barbut, H. Kadau, M. Schmitt, M. Wenzel, and T. Pfau, Observation of quantum droplets in a strongly dipolar Bose gas, *Phys. Rev. Lett.* **116**, 215301 (2016).
- [8] L. Chomaz, D. Petter, P. Ilzhöfer, G. Natale, A. Trautmann, C. Politi, G. Durastante, R. M. W. van Bijnen, A. Patscheider, M. Sohmen, M. J. Mark, and F. Ferlaino, Long-lived and transient supersolid behaviors in dipolar quantum gases, *Phys. Rev. X* **9**, 021012 (2019).
- [9] L. Tanzi, E. Lucioni, F. Famà, J. Catani, A. Fioretti, C. Gabbanini, R. N. Bisset, L. Santos, and G. Modugno, Observation of a dipolar quantum gas with metastable supersolid properties, *Phys. Rev. Lett.* **122**, 130405 (2019).

- [10] F. Böttcher, J.-N. Schmidt, M. Wenzel, J. Hertkorn, M. Guo, T. Langen, and T. Pfau, Transient supersolid properties in an array of dipolar quantum droplets, *Phys. Rev. X* **9**, 011051 (2019).
- [11] M. Sohmen, C. Politi, L. Klaus, L. Chomaz, M. J. Mark, M. A. Norcia, and F. Ferlaino, Birth, life, and death of a dipolar supersolid, *Phys. Rev. Lett.* **126**, 233401 (2021).
- [12] J. Sánchez-Baena, C. Politi, F. Maucher, F. Ferlaino, and T. Pohl, Heating a dipolar quantum fluid into a solid, *Nat. Commun.* **14**, 1868 (2023).
- [13] L. Chomaz, R. M. W. van Bijnen, D. Petter, G. Faraoni, S. Baier, J. H. Becher, M. J. Mark, F. Wächtler, L. Santos, and F. Ferlaino, Observation of roton mode population in a dipolar quantum gas, *Nat. Phys.* **14**, 442 (2018).
- [14] I. Ferrier-Barbut, M. Wenzel, F. Böttcher, T. Langen, M. Isoard, S. Stringari, and T. Pfau, Scissors mode of dipolar quantum droplets of dysprosium atoms, *Phys. Rev. Lett.* **120**, 160402 (2018).
- [15] L. Tanzi, J. G. Maloberti, G. Biagioni, A. Fioretti, C. Gabbanini, and G. Modugno, Evidence of superfluidity in a dipolar supersolid from nonclassical rotational inertia, *Science* **371**, 1162 (2021).
- [16] L. Tanzi, S. M. Rocuzzo, E. Lucioni, F. Famà, A. Fioretti, C. Gabbanini, G. Modugno, A. Recati, and S. Stringari, Supersolid symmetry breaking from compressional oscillations in a dipolar quantum gas, *Nature (London)* **574**, 382 (2019).
- [17] J.-N. Schmidt, J. Hertkorn, M. Guo, F. Böttcher, M. Schmidt, K. S. H. Ng, S. D. Graham, T. Langen, M. Zwierlein, and T. Pfau, Roton excitations in an oblate dipolar quantum gas, *Phys. Rev. Lett.* **126**, 193002 (2021).
- [18] J. Hertkorn, J.-N. Schmidt, F. Böttcher, M. Guo, M. Schmidt, K. S. H. Ng, S. D. Graham, H. P. Büchler, T. Langen, M. Zwierlein, and T. Pfau, Density fluctuations across the superfluid-supersolid phase transition in a dipolar quantum gas, *Phys. Rev. X* **11**, 011037 (2021).
- [19] N. Bigagli, W. Yuan, S. Zhang, B. Bulatovic, T. Karman, I. Stevenson, and S. Will, Observation of Bose-Einstein condensation of dipolar molecules, [arXiv:2312.10965](https://arxiv.org/abs/2312.10965).
- [20] R. Schützhold, M. Uhlmann, Y. Xu, and U. R. Fischer, Mean-field expansion in Bose-Einstein condensates with finite-range interactions, *Int. J. Mod. Phys. B* **20**, 3555 (2006).
- [21] A. R. P. Lima and A. Pelster, Quantum fluctuations in dipolar Bose gases, *Phys. Rev. A* **84**, 041604(R) (2011).
- [22] A. R. P. Lima and A. Pelster, Beyond mean-field low-lying excitations of dipolar Bose gases, *Phys. Rev. A* **86**, 063609 (2012).
- [23] D. Baillie, R. M. Wilson, R. N. Bisset, and P. B. Blakie, Self-bound dipolar droplet: A localized matter wave in free space, *Phys. Rev. A* **94**, 021602(R) (2016).
- [24] R. N. Bisset, R. M. Wilson, D. Baillie, and P. B. Blakie, Ground-state phase diagram of a dipolar condensate with quantum fluctuations, *Phys. Rev. A* **94**, 033619 (2016).
- [25] F. Wächtler and L. Santos, Ground-state properties and elementary excitations of quantum droplets in dipolar Bose-Einstein condensates, *Phys. Rev. A* **94**, 043618 (2016).
- [26] H. Saito, Path-integral Monte Carlo study on a droplet of a dipolar Bose-Einstein condensate stabilized by quantum fluctuation, *J. Phys. Soc. Jpn.* **85**, 053001 (2016).
- [27] Y.-C. Zhang, F. Maucher, and T. Pohl, Supersolidity around a critical point in dipolar Bose-Einstein condensates, *Phys. Rev. Lett.* **123**, 015301 (2019).
- [28] P. B. Blakie, D. Baillie, L. Chomaz, and F. Ferlaino, Supersolidity in an elongated dipolar condensate, *Phys. Rev. Res.* **2**, 043318 (2020).
- [29] R. N. Bisset, L. A. Peña Ardila, and L. Santos, Quantum droplets of dipolar mixtures, *Phys. Rev. Lett.* **126**, 025301 (2021).
- [30] G. Natale, R. M. W. van Bijnen, A. Patscheider, D. Petter, M. J. Mark, L. Chomaz, and F. Ferlaino, Excitation spectrum of a trapped dipolar supersolid and its experimental evidence, *Phys. Rev. Lett.* **123**, 050402 (2019).
- [31] M. Wenzel, F. Böttcher, J.-N. Schmidt, M. Eisenmann, T. Langen, T. Pfau, and I. Ferrier-Barbut, Anisotropic superfluid behavior of a dipolar Bose-Einstein condensate, *Phys. Rev. Lett.* **121**, 030401 (2018).
- [32] M. Wenzel, F. Böttcher, T. Langen, I. Ferrier-Barbut, and T. Pfau, Striped states in a many-body system of tilted dipoles, *Phys. Rev. A* **96**, 053630 (2017).
- [33] D. Petter, G. Natale, R. M. W. van Bijnen, A. Patscheider, M. J. Mark, L. Chomaz, and F. Ferlaino, Probing the roton excitation spectrum of a stable dipolar Bose gas, *Phys. Rev. Lett.* **122**, 183401 (2019).
- [34] F. Böttcher, M. Wenzel, J.-N. Schmidt, M. Guo, T. Langen, I. Ferrier-Barbut, T. Pfau, R. Bombín, J. Sánchez-Baena, J. Boronat, and F. Mazzanti, Dilute dipolar quantum droplets beyond the extended Gross-Pitaevskii equation, *Phys. Rev. Res.* **1**, 033088 (2019).
- [35] A. Y. Cherny, Low-density expansions for the homogeneous dipolar Bose gas at zero temperature, *Phys. Rev. A* **100**, 063631 (2019).
- [36] A. Boudjemâa and N. Guebli, Quantum correlations in dipolar droplets: Time-dependent Hartree-Fock-Bogoliubov theory, *Phys. Rev. A* **102**, 023302 (2020).
- [37] F. Zhang and L. Yin, Phonon stability of quantum droplets in dipolar Bose gases, *Chin. Phys. Lett.* **39**, 060301 (2022).
- [38] A. Boudjemâa, Properties of dipolar bosonic quantum gases at finite temperatures, *J. Phys. A* **49**, 285005 (2016).
- [39] A. Boudjemâa, Quantum dilute droplets of dipolar bosons at finite temperature, *Ann. Phys. (NY)* **381**, 68 (2017).
- [40] A. Macia, J. Sánchez-Baena, J. Boronat, and F. Mazzanti, Droplets of trapped quantum dipolar bosons, *Phys. Rev. Lett.* **117**, 205301 (2016).
- [41] R. Bombín, F. Mazzanti, and J. Boronat, Off-diagonal long-range order in arrays of dipolar droplets, *New J. Phys.* **26**, 013052 (2024).
- [42] V. Cikojević, L. V. Markić, M. Pi, M. Barranco, and J. Boronat, Towards a quantum Monte Carlo-based density functional including finite-range effects: Excitation modes of a ^{39}K quantum droplet, *Phys. Rev. A* **102**, 033335 (2020).
- [43] V. Cikojević, L. V. Markić, and J. Boronat, Finite-range effects in ultradilute quantum drops, *New J. Phys.* **22**, 053045 (2020).
- [44] V. Cikojević, E. Poli, F. Ancilotto, L. Vranješ-Markić, and J. Boronat, Dilute quantum liquid in a K-Rb Bose mixture, *Phys. Rev. A* **104**, 033319 (2021).
- [45] J. Kopyciński, L. Parisi, N. G. Parker, and K. Pawłowski, Quantum Monte Carlo-based density functional for one-dimensional Bose-Bose mixtures, *Phys. Rev. Res.* **5**, 023050 (2023).
- [46] F. Ancilotto, M. Barranco, F. Coppens, J. Eloranta, N. Halberstadt, A. Hernando, D. Mateo, and M. Pi, Density

- functional theory of doped superfluid liquid helium and nanodroplets, *Int. Rev. Phys. Chem.* **36**, 621 (2017).
- [47] M. Barranco, R. Guardiola, S. Hernández, R. Mayol, J. Navarro, and M. Pi, Helium nanodroplets: An overview, *J. Low Temp. Phys.* **142**, 1 (2006).
- [48] H. Li, J.-F. Wyart, O. Dulieu, S. Nascimbène, and M. Lepers, Optical trapping of ultracold dysprosium atoms: Transition probabilities, dynamic dipole polarizabilities and van der Waals C6 coefficients, *J. Phys. B* **50**, 014005 (2017).
- [49] D. M. Ceperley, Path integrals in the theory of condensed helium, *Rev. Mod. Phys.* **67**, 279 (1995).
- [50] A. Sarsa, K. E. Schmidt, and W. R. Magro, A path integral ground state method, *J. Chem. Phys.* **113**, 1366 (2000).
- [51] D. E. Galli and L. Reatto, Recent progress in simulation of the ground state of many boson systems, *Mol. Phys.* **101**, 1697 (2003).
- [52] J. E. Cuervo, P.-N. Roy, and M. Boninsegni, Path integral ground state with a fourth-order propagator: Application to condensed helium, *J. Chem. Phys.* **122**, 114504 (2005).
- [53] S. A. Chin, Quantum statistical calculations and symplectic corrector algorithms, *Phys. Rev. E* **69**, 046118 (2004).
- [54] S. A. Chin, Complete characterization of fourth-order symplectic integrators with extended-linear coefficients, *Phys. Rev. E* **73**, 026705 (2006).
- [55] N. Prokof'ev, B. Svistunov, and I. Tupitsyn, "Worm" algorithm in quantum Monte Carlo simulations, *Phys. Lett. A* **238**, 253 (1998).
- [56] M. Boninsegni, N. Prokof'ev, and B. Svistunov, Worm algorithm for continuous-space path integral Monte Carlo simulations, *Phys. Rev. Lett.* **96**, 070601 (2006).
- [57] R. Rota, J. Casulleras, F. Mazzanti, and J. Boronat, High-order time expansion path integral ground state, *Phys. Rev. E* **81**, 016707 (2010).
- [58] F. Ancilotto, M. Barranco, M. Guilleumas, and M. Pi, Self-bound ultradilute Bose mixtures within local density approximation, *Phys. Rev. A* **98**, 053623 (2018).
- [59] M. Guo, F. Böttcher, J. Hertkorn, J.-N. Schmidt, M. Wenzel, H. P. Büchler, T. Langen, and T. Pfau, The low-energy goldstone mode in a trapped dipolar supersolid, *Nature (London)* **574**, 386 (2019).
- [60] P. Ilzhöfer, M. Sohmen, G. Durastante, C. Politi, A. Trautmann, G. Natale, G. Morpurgo, T. Giamarchi, L. Chomaz, M. J. Mark, and F. Ferlaino, Phase coherence in out-of-equilibrium supersolid states of ultracold dipolar atoms, *Nat. Phys.* **17**, 356 (2021).
- [61] A. J. Leggett, Can a solid be "superfluid"? *Phys. Rev. Lett.* **25**, 1543 (1970).
- [62] R. Ghosh, C. Mishra, L. Santos, and R. Nath, Droplet arrays in doubly dipolar Bose-Einstein condensates, *Phys. Rev. A* **106**, 063318 (2022).
- [63] G. Chauveau, C. Maury, F. Rabec, C. Heintze, G. Brochier, S. Nascimbene, J. Dalibard, J. Beugnon, S. M. Roccuzzo, and S. Stringari, Superfluid fraction in an interacting spatially modulated Bose-Einstein condensate, *Phys. Rev. Lett.* **130**, 226003 (2023).
- [64] J. Lin, G. Chen, M. Jin, Z. Shi, F. Deng, W. Zhang, G. Quémener, T. Shi, S. Yi, and D. Wang, Microwave shielding of bosonic NaRb molecules, *Phys. Rev. X* **13**, 031032 (2023).
- [65] N. Bigagli, C. Warner, W. Yuan, S. Zhang, I. Stevenson, T. Karman, and S. Will, Collisionally stable gas of bosonic dipolar ground-state molecules, *Nat. Phys.* **19**, 1579 (2023).
- [66] M. Schmidt, L. Lassablière, G. Quémener, and T. Langen, Self-bound dipolar droplets and supersolids in molecular Bose-Einstein condensates, *Phys. Rev. Res.* **4**, 013235 (2022).
- [67] B. Mukherjee, M. D. Frye, C. R. Le Sueur, M. R. Tarbutt, and J. M. Hutson, Shielding collisions of ultracold CaF molecules with static electric fields, *Phys. Rev. Res.* **5**, 033097 (2023).
- [68] F. Deng, X.-Y. Chen, X.-Y. Luo, W. Zhang, S. Yi, and T. Shi, Effective potential and superfluidity of microwave-shielded polar molecules, *Phys. Rev. Lett.* **130**, 183001 (2023).
- [69] V. Cikojevic, Critical atom number notebook, 2023, <https://github.com/viktorcikojevic/dipolar-droplets>.